Chapter 4
Vertical Discretizations: Some Basic Ideas

John Thuburn

Abstract This chapter introduces some key ideas in the design of vertical discretizations for atmospheric models. Various choices of vertical coordinate are possible, and the most widely used ones are introduced. The requirement to retain certain conservation properties can constrain or determine aspects of the discretization: this is illustrated using the Simmons and Burridge angular momentum and energy conserving scheme for hydrostatic models. Another important set of issues surrounds the ability to capture hydrostatic balance and wave dispersion accurately and to avoid computational modes: some implications for the vertical discretization are discussed.

4.1 Introduction

This lecture will introduce some key, basic ideas related to vertical discretizations in atmospheric model dynamical cores. We will first discuss the choice of vertical coordinate and its relation to the bottom and top boundary conditions. We will then look at how the details of the vertical discretization can influence conservation properties and wave propagation.

4.2 Alternative Vertical Coordinates

Systematic derivation of the governing equations usually involves writing their components in some orthogonal coordinate system, such as spherical polars (λ, ϕ, r). However, for numerical solution of the equations there may be advantages to

J. Thuburn
School of Engineering, Computing and Mathematics, University of Exeter, North Park Road, Exeter, EX4 4QF, UK
e-mail: j.thuburn@ex.ac.uk

P.H. Lauritzen et al. (eds.), *Numerical Techniques for Global Atmospheric Models*, Lecture Notes in Computational Science and Engineering 80,
DOI 10.1007/978-3-642-11640-7_4,

writing the equations in terms of some alternative vertical coordinate. The following transformation rules (e.g., Kasahara 1974; Staniforth and Wood 2003) allow us to re-express the horizontal and vertical derivatives and hence transform the equations to an arbitrary vertical coordinate $\eta(\lambda, \phi, r, t)$:

$$\frac{\partial \psi}{\partial r} = \frac{\partial \eta}{\partial r} \frac{\partial \psi}{\partial \eta}, \tag{4.1}$$

$$\left(\frac{\partial \psi}{\partial s}\right)_r = \left(\frac{\partial \psi}{\partial s}\right)_\eta + \left(\frac{\partial \psi}{\partial \eta}\right)\left(\frac{\partial \eta}{\partial s}\right)_r, \tag{4.2}$$

$$\frac{D\psi}{Dt} = \frac{\partial \psi}{\partial t} + \mathbf{v}.\nabla_{\mathrm{H}}\psi + \dot{\eta}\frac{\partial \psi}{\partial \eta}. \tag{4.3}$$

Here s may be λ, ϕ or t, and ∇_{H} is the horizontal gradient at constant η.

In transforming to a different vertical coordinate it is usual to continue to express vectors in terms of their components in the original orthogonal coordinate system, rather than transform to covariant or contravariant components in the new coordinate system. In particular, it is usual to retain the velocity components $u = \dot{\lambda} r \cos\phi$, $v = \dot{\phi} r$, $w = \dot{r}$ (though $\dot{\eta}$ may be needed too).

4.2.1 Examples

- *Height* $\eta = r$ or $\eta = z$. This is the most obvious choice, requiring no transformation of the governing equations.
- *Pressure* $\eta = p$. A pressure-based coordinate is particularly attractive in hydrostatic models because the mass continuity equation becomes purely diagnostic, and because the pressure difference across a layer is proportional to the mass per unit area in that layer (under the shallow atmosphere approximation), making it easier to formulate schemes with desired conservation properties.
- *Mass* $\eta = \int_z^\infty \rho \, dz'$ for Cartesian geometry with height z or $\eta = \int_r^\infty \rho r'^2 \, dr'$ with distance r from Earth's centre. This is the natural generalization of the pressure coordinate to non-hydrostatic models.
- *Terrain-following variants*. It is possible to modify the three coordinate systems mentioned above so that the ground becomes a coordinate surface (e.g., Phillips 1957; Gal-Chen and Somerville 1975, Fig. 4.1); this greatly simplifies the application of the bottom boundary condition (see Sect. 4.3). Some examples are $\eta = z - z_s$ where z_s is the height of the ground, or $\eta = p/p_s$ where p_s is the surface pressure. This latter is sometimes called a σ coordinate.
- *Hybrid terrain-following variants*. To avoid numerical artefacts at high altitudes resulting from a terrain following coordinate, it is possible to use a hybrid coordinate that is terrain-following near the ground but returns to a height or pressure coordinate at high altitude (Fig. 4.1). One well known example is the hybrid σ-p coordinate introduced by Simmons and Burridge (1981). A value of a and a value of b are defined on each model level. Then the pressure on each model level is

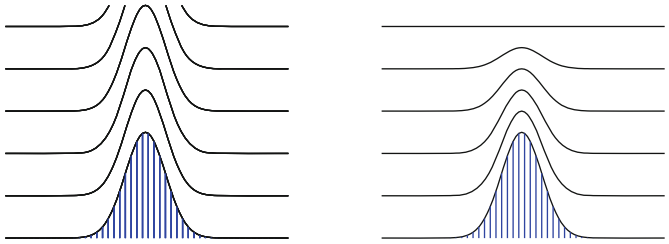

Fig. 4.1 Schematics showing a terrain following coordinate (*left*) and a hybrid terrain following coordinate (*right*)

given by $p = ap_0 + bp_s$ where p_0 is a constant reference pressure and p_s is again the surface pressure. Near the ground a is chosen to be zero or small so that the coordinate looks like a σ coordinate; at high altitude b is chosen to be zero or small so that the coordinate looks like a pressure coordinate. The coefficients are chosen to give a smooth transition in between. (A value of η is given by $\eta = a + b$, though in fact the scheme can be formulated without explicit reference to the value of η.)

- *Isentropic coordinate* $\eta = f(\theta)$. There are a number of potential advantages of using an isentropic vertical coordinate that make it attractive for atmospheric modeling (e.g., Hsu and Arakawa 1990). Diabatic heating is generally weak, so an isentropic coordinate is approximately Lagrangian, leading to improved Lagrangian conservation properties and conservation of entropy-related quantities and perhaps potential vorticity. The handling of moist processes may also be improved. And in some dynamical situations the coordinate automatically adapts to give extra resolution where it is needed. On the other hand, the bottom boundary is difficult to handle, the coordinate cannot handle situations where $N^2 < 0$, and experience suggests it is more difficult to obtain a robust numerical formulation. (A hybrid vertical coordinate can help with all of these issues, e.g., Konor and Arakawa 1997). Also, in regions such as the tropical upper troposphere, where N^2 is close to zero, vertical resolution becomes relatively poor.
- *Lagrangian coordinate*. A Lagrangian vertical coordinate (apparently first suggested by Starr 1945) is defined by $\dot{\eta} = 0$. Like the isentropic coordinate, it is expected to give improved Lagrangian conservation properties. However, over time Lagrangian coordinate surfaces will bend and fold, making them inaccurate or unusable as a vertical coordinate. To circumvent this, the Lagrangian coordinate must be periodically re-initialized and the solution remapped to the re-initialized coordinate system (e.g., Lin 2004).

4.3 Bottom and Top Boundary Conditions

The normal component of velocity at the bottom boundary must vanish. If η is a terrain following coordinate then the boundary condition may be expressed particularly simply as $\dot{\eta} = 0$. In terms of velocity components we must have $w = \mathbf{v}.\nabla_H z_s$,

where $\mathbf{v} = (u, v)$ is the horizontal velocity. If the ground is flat then we have $w = 0$, but not in general. Typically w will be stored at the bottom boundary, but u and v will be staggered in the vertical relative to w (see Sect. 4.5). Thus, some means of evaluating $\mathbf{v}$ at the gound will be needed. If the model includes a boundary layer scheme then it is appropriate to apply a no-slip boundary condition $\mathbf{v} = 0$, and it again follows that $w = 0$. However, for a frictionless dynamical core a free-slip boundary condition, which imposes no constraint on $\mathbf{v}$, is more appropriate; then $\mathbf{v}$ must be extrapolated to the ground in a way consistent with the free-slip condition.

A disadvantage of terrain-following coordinates, particularly at high horizontal resolution, is that the coordinate system becomes far from orthogonal near steep orography. Numerical methods can then lose accuracy. To avoid this problem, an alternative is not to use a terrain-following coordinate but to retain a height coordinate and allow the coordinate surfaces to intersect the terrain.

In the simplest version of this idea the orography appears step-like, with the top of each step coincident with a model coordinate surface (Fig. 4.2). This has been found to be too inaccurate. However, the idea can be extended (e.g., Adcroft et al. 1997) by allowing the bottom face of grid cells adjacent to the gound to be at any height, not necessarily coincident with a model coordinate surface (*fractional cells*), or even allowing them to slope (*cut cells* or *shaved cells*). A disadvantage remains that vertical resolution in the boundary layer becomes reduced at mountain tops as model grids are typically vertically stretched at higher altitudes.

The real atmosphere has no top boundary, but in a practical numerical model of the atmosphere we must impose a boundary somewhere. Practical choices include the following (e.g., Staniforth and Wood 2003).

- *Rigid lid*: $w = 0$ is imposed at some constant height $z = z_T$. This is most easily done if the vertical coordinate is height (or a hybrid coordinate reducing to height near the top boundary). Conservation of energy and angular momentum are maintained in the governing equations.
- *Elastic lid*: $Dp/Dt = 0$ is imposed on some surface of constant pressure $p = p_T$. (p_T may equal 0.) This is most easily done if the vertical coordinate is pressure (or a hybrid coordinate reducing to pressure near the top boundary). The governing equations then conserve angular momentum and enthalpy.

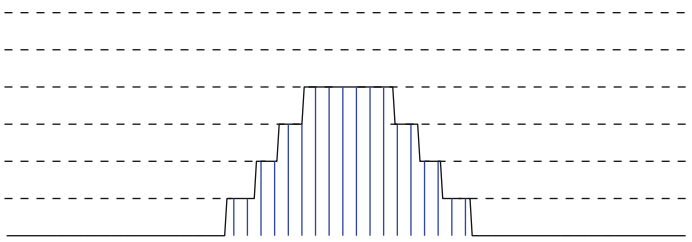

Fig. 4.2 Schematic showing the simplest form of terrain intersecting vertical coordinate

Both a rigid lid and an elastic lid are artificial and may cause spurious reflection of upward propagating waves. To reduce the problem it is common to include a scale-independent damping on model fields near the model top, but note that the strength and depth of the damping layer must be chosen carefully. Moreover, it is recommended that such damping only be applied to departures from the zonal mean to avoid an unrealistic sink of angular momentum and spurious feedbacks (Shaw and Shepherd 2007). An alternative is to apply a wave radiation condition at the model top (e.g., Durran 1999). However, this approach is more complex and some approximation is usually required.

4.4 The Simmons and Burridge Energy and Angular Momentum Conserving Scheme

In this section we use the well-known Simmons and Burridge (1981) vertical discretization to illustrate the kinds of considerations that come into play to obtain properties such as conservation of energy and angular momentum. It is assumed that the hydrostatic primitive equations are being solved, and a hybrid $\sigma - p$ coordinate is used. Figure 4.3 shows the vertical arrangement of variables: the pressure, and the vertical coordinate η if needed, are defined on 'half-levels', while the prognostic variables u, v and T are defined at the 'full-levels'. We suppose there are N full-levels, numbered from the top (where $\eta = 0$) to the bottom (where $\eta = 1$). Surface pressure (or log of surface pressure) is predicted at the ground, which is the half-level with index $N + 1/2$.

4.4.1 Hydrostatic Equation

We first look at the discretization of the hydrostatic equation

$$\frac{\partial \Phi}{\partial \eta} = -\frac{RT}{p}\frac{\partial p}{\partial \eta}. \tag{4.4}$$

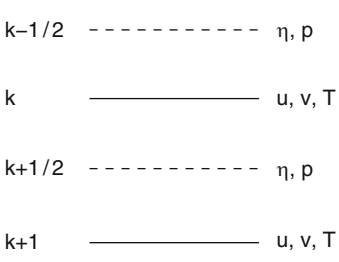

Fig. 4.3 Schematic showing the vertical arrangement of variables for the Simmons and Burridge scheme. k is the level index

Here Φ is the geopotential and R is the gas constant for dry air. This is naturally discretized as

$$\Phi_{k+1/2} - \Phi_{k-1/2} = -RT_k \ln \frac{p_{k+1/2}}{p_{k-1/2}}. \tag{4.5}$$

Since Φ at the ground is given, if we know the half-level pressures and the full-level temperatures then we can easily integrate (4.5) to obtain Φ at any half-level.

However, Φ is required in the momentum equations at full-levels. Therefore a further contribution proportional to T_k is added to obtain full-level values of Φ:

$$\Phi_k = \Phi_{k+1/2} + \alpha_k R T_k. \tag{4.6}$$

We have some freedom in exactly how the α's are specified; see Simmons and Burridge (1981) for a specific example. Here we will not specify α but keep the discussion as general as possible. Note that α_k may depend on $p_{k-1/2}$ and $p_{k+1/2}$ and hence on p_s.

Note that this scheme supports a *computational mode*: for any given hydrostatically balanced profile of T_k, p_s, and Φ_k, we can find a pattern of T and p_s perturbations that, when added to the original profile, has no effect on the Φ_k. Such a perturbation profile is therefore invisible to the dynamics. See Sect. 4.5.2 for further discussion.

4.4.2 Angular Momentum Conservation

The vertical coordinate defines the pressure at the half-levels. However, for the momentum equation we require the horizontal pressure gradient at the full-levels. Demanding angular momentum conservation tells us how we should define the full-level pressure gradient.

In spherical coordinates, the equation for the eastward velocity component is

$$\frac{Du}{Dt} - \frac{uv\tan\phi}{a} - fv + \frac{1}{a\cos\phi}\frac{\partial\Phi}{\partial\lambda} + \frac{RT}{p}\frac{1}{a\cos\phi}\frac{\partial p}{\partial\lambda} = 0, \tag{4.7}$$

where a is the Earth's radius. Multiplying by $a\cos\phi$ and using $a\,D\phi/Dt = v$ gives an equation for the angular momentum density $m = ua\cos\phi + a^2\Omega\cos^2\phi$:

$$\frac{Dm}{Dt} + \frac{\partial\Phi}{\partial\lambda} + \frac{RT}{p}\frac{\partial p}{\partial\lambda} = 0. \tag{4.8}$$

The net source of angular momentum, integrated over a latitudinal slice, is

$$\begin{aligned}&\int_0^{2\pi}\int_0^1 \left(\frac{\partial\Phi}{\partial\lambda} + \frac{RT}{p}\frac{\partial p}{\partial\lambda}\right)\frac{\partial p}{\partial\eta}\,d\eta\,d\lambda \\ &= \int_0^{2\pi}\int_0^1 \left(\frac{\partial\Phi}{\partial\lambda}\frac{\partial p}{\partial\eta} - \frac{\partial\Phi}{\partial\eta}\frac{\partial p}{\partial\lambda}\right)d\eta\,d\lambda\end{aligned}$$

$$= \int_0^{2\pi} \int_0^1 \frac{\partial}{\partial \eta} \left(-\Phi \frac{\partial p}{\partial \lambda} \right) + \frac{\partial}{\partial \lambda} \left(\Phi \frac{\partial p}{\partial \eta} \right) d\eta \, d\lambda$$

$$= -\int_0^{2\pi} \Phi_s \frac{\partial p_s}{\partial \lambda} \, d\lambda, \tag{4.9}$$

where Φ_s is the surface geopotential, and we have used the hydrostatic relation and the boundary conditions to simplify the integral. Repeating this derivation for the finite difference scheme, we find that a finite difference analogue of this formula will hold provided

$$\sum_{k=1}^{N} \Phi_k \frac{\partial}{\partial \lambda} \Delta p_k = \Phi_s \frac{\partial p_s}{\partial \lambda} + \sum_{k=1}^{N} R \left(\frac{T}{p} \frac{\partial p}{\partial \lambda} \right)_k \Delta p_k, \tag{4.10}$$

which, in turn, will hold provided we define the full-level pressure gradient via

$$\left(\frac{RT}{p} \nabla p \right)_k = \frac{RT_k}{\Delta p_k} \left[\left(\ln \frac{p_{k+1/2}}{p_{k-1/2}} \right) \nabla p_{k-1/2} + \alpha_k \nabla (\Delta p_k) \right], \tag{4.11}$$

where α_k is the same as used in (4.6) to define the full-level Φ.

4.4.3 Energy Conservation

Taking $\mathbf{v}$ times the momentum equation gives

$$\frac{D}{Dt} \left(\frac{\mathbf{v}^2}{2} \right) = -\mathbf{v}.\nabla \Phi - \frac{RT}{p} \mathbf{v}.\nabla p, \tag{4.12}$$

while the thermodynamic equation may be written

$$\frac{D}{Dt} c_p T = \frac{RT\omega}{p}, \tag{4.13}$$

where

$$\omega \equiv \frac{Dp}{Dt} = -\int_0^{\eta} \nabla. \left(\mathbf{v} \frac{\partial p}{\partial \eta} \right) d\eta + \mathbf{v}.\nabla p. \tag{4.14}$$

The terms on the right hand sides of (4.12) and (4.13) represent conversions between kinetic and potential or internal energy. The global integral of the sum of the conversion terms vanishes, implying energy conservation.

For the discretization we need to define ω at full-levels using a finite-difference analogue of (4.14). It may be verified that if we evaluate RT/p times the vertical integral term as

$$\frac{RT_k}{\Delta p_k}\left[\left(\ln\frac{p_{k+1/2}}{p_{k-1/2}}\right)\sum_{r=1}^{k-1}\nabla.(\mathbf{v}_r\,\Delta p_r)+\alpha_k\nabla.(\mathbf{v}_k\,\Delta p_k)\right] \tag{4.15}$$

and evaluate $(RT/p)\nabla p$ using (4.11) as in the momentum equation then all contributions to the global integral of the conversion terms do indeed cancel and so the scheme preserves energy conservation.

The expressions (4.11) and (4.15) are not the most obvious finite difference discretizations of the corresponding continuous expressions; it is typically non-trivial to obtain such conservation properties.

4.5 Wave Dispersion and Balance

In Chap. 3 we saw how different choices of horizontal grid staggering (and prognostic variables) can affect the accuracy with which we capture the propagation of different classes of waves, particularly short wavelength waves that are marginally resolved. Accurate representation of the propagation of fast waves is important for capturing adjustment towards balance, and hence for capturing balanced motions themselves. Similar issues arise when considering vertical discretizations.

4.5.1 The Lorenz and Charney–Phillips Grids

For models solving the hydrostatic equations we have three-dimensional fields of three prognostic variables: usually the two horizontal wind components (or some equivalent information in terms of vorticy and divergence) and a thermodynamic variable. (In some formulations we also have a surface pressure field.) Two classes of vertical grid are widely used for hydrostatic models: those in which the thermodynamic variable is stored at the same levels as the wind variables, and those in which the thermodynamic variable is staggered in the vertical relative to the wind variables. These are commonly referred to as the Lorenz grids and Charney–Phillips grids, respectively, (Fig. 4.4) after Lorenz (1960) and Charney and Phillips (1953).

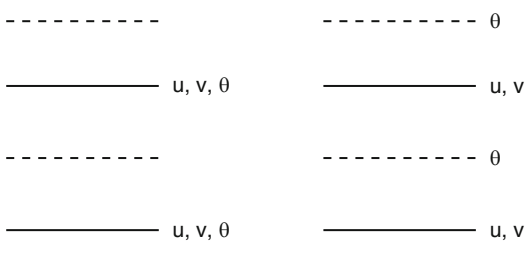

Fig. 4.4 Schematic showing the vertical arrangement of variables for the Lorenz (*left*) and Charney–Phillips (*right*) grids

4.5.2 Lorenz Grid Computational Mode

One well-known drawback of the Lorenz grids is that they support a *computational mode*. Consider, for example, the Simmons and Burridge scheme discussed above. Suppose we have vertical profiles of T, p_s and Φ satisfying hydrostatic balance (4.5). Now consider making some perturbations T'_k to the temperature values and p'_s to the surface pressure; through the linearized version of (4.5), these will imply corresponding perturbations Φ'_k in the geopotential. The geopotential perturbation at the lowest full-level is

$$\Phi'_N = \alpha_N R T'_N + R T_N \frac{d\alpha_N}{dp_s} p'_s, \tag{4.16}$$

while the difference between successive full-level geopotential perturbations is

$$\begin{aligned} \Phi'_k - \Phi'_{k-1} = {} & R \left\{ \alpha_k + \ln \left(\frac{p_{k+1/2}}{p_{k-1/2}} \right) \right\} T'_k \\ & - R\alpha_{k-1} T'_{k-1} \\ & + \left\{ R T_k \left(\frac{d\alpha_k}{dp_s} + \frac{b_{k+1/2}}{p_{k+1/2}} - \frac{b_{k-1/2}}{p_{k-1/2}} \right) - R T_{k-1} \frac{d\alpha_{k-1}}{dp_s} \right\} p'_s, \end{aligned} \tag{4.17}$$

where $b_{k+1/2} = dp_{k+1/2}/dp_s$.

For an arbitrary p'_s, we can ensure that Φ'_N vanishes by a suitable choice of T'_N. But then we can ensure that Φ'_{N-1} vanishes by a suitable choice of T'_{N-1}, and so on. In this way we can find a profile of T'_k such that all Φ'_k vanish. Such a p'_s and T'_k profile will therefore have no effect on the momentum equation; it will be invisible to the dynamics and will not propagate (Tokioka 1978; Arakawa and Moorthi 1988). The key point here is that there is one more degree of freedom in $\{T_k, k = 1, ..., N; p_s\}$ than there is in $\{\Phi_k, k = 1, ..., N\}$; basic linear algebra then implies that there exists a family of nonzero solutions for $\{T'_k, k = 1, ..., N; p'_s\}$ that make $\{\Phi'_k, k = 1, ..., N\}$ vanish.

Related to the existence of the computational mode is the possibility of a spurious resonant response to a steady thermal forcing. If the forcing projects onto the computational mode then the response will grow linearly with time (until nonlinear effects come into play) rather than reaching a steady response (Schneider 1987).

4.5.3 Compressible Euler Equations

The compressible Euler equations do not make the hydrostatic approximation or any kind of incompressibility approximation; they therefore support acoustic waves as well as inertio-gravity and Rossby waves. For the compressible Euler equations we have five prognostic variables, usually three velocity variables and

two thermodynamic variables. There are therefore many different possibilities for choosing staggered grids. There are also different possible choices for which thermodynamic variables are predicted, e.g., any two from ρ, p, T, θ, etc. In this subsection we will restrict attention to the use of height z as the vertical coordinate with a uniform grid spacing Δz, but similar reasoning applies to other vertical coordinates (Thuburn and Woollings 2005; Thuburn 2006).

Numerical exploration of a large number of possible configurations (Thuburn and Woollings 2005) shows that:

- Accurate representation of acoustic waves is necessary (but not sufficient) for an accurate representation of inertio-gravity waves
- Which in turn is necessary (but not sufficient) for an accurate representation of Rossby waves

Here, by considering the dispersion relations for different kinds of waves, we attempt to give heuristic explanations for the kinds of configuration that give the best representation of wave propagation. Just as we found when considering horizontal discretizations, we want to avoid or minimize taking averages, and we want to avoid or minimize taking differences over $2\Delta z$, since these approximations introduce large errors in the propagation of short waves.

In what follows we will consider wavelike solutions of the governing equations with wavevector (k, l, m) and frequency ω. Also define the total horizontal wavenumber squared $K^2 = k^2 + l^2$, the gravitational acceleration g, the Coriolis parameter f, and the buoyancy frequency N.

4.5.3.1 Acoustic Waves

The acoustic wave dispersion relation is

$$\omega^2 \approx (m^2 + K^2)c^2, \tag{4.18}$$

where c is the speed of sound. Here, one factor of m comes from the vertical derivative of p appearing in the w equation, and the other comes from the vertical derivative of w appearing in the p equation. Thus, we will capture the dispersion relation as accurately as possible if we capture these two vertical derivatives as accurately as possible in the limit of short vertical wavelength. We therefore require:

- $\delta_z p$ at the same level as w
- $\delta_z w$ at the same level as p

where δ_z represents a finite difference approximation to $\partial/\partial z$. This implies that p should be staggered with respect to w to obtain the most compact finite difference approximations.

If p is not predicted but ρ is, then, for vertical-grid-scale waves, p perturbations (expressed in terms of the two predicted thermodynamic variables) will be dominated by ρ perturbations provided $\Delta z \ll g/N^2$, which will always hold in practice; this then implies that ρ should be staggered with respect to w.

4.5.3.2 Inertio-Gravity Waves

The inertio-gravity wave dispersion relation is

$$\omega^2 \approx \frac{m^2 f^2 + K^2 N^2}{m^2 + K^2}. \tag{4.19}$$

The denominator arises in the same way as the $m^2 + K^2$ factor in the acoustic wave dispersion relation and so again will be captured as accurately as possible provided p (or ρ) is staggered with respect to w. The m^2 term in the numerator also arises in the same way, yet again requiring p (or ρ) staggered with respect to w. Depending on the horizontal wavelength and on the relative sizes of f and N, it is possible that the K^2N^2 term in the numerator could dominate even for the shortest resolved vertical wavelengths. To capture the K^2N^2 term accurately requires that u and v be stored at the same levels as p in order to capture the pressure gradient term in the horizontal momentum equations without averaging, and also requires that the buoyancy variable (e.g., the potential temperature θ) be stored at the same levels as w in order to capture the buoyancy source due to vertical advection and the effect of buoyancy in the w equation without averaging.

If we do not predict θ but predict, say, T and p or T and ρ then there are comparable contributions to the θ perturbation from the two predicted thermodynamic variables. Optimal wave propagation would then require both p or ρ staggered with respect to w (to capture the $m^2 f^2$ term) *and* p or ρ collocated with w (to capture the K^2N^2 term), which is obviously not possible. In other words, optimal wave propagation requires that we predict θ or some function of θ.

4.5.3.3 Rossby Waves

The Rossby wave dispersion relation is

$$\omega \approx -\frac{k\beta N^2}{m^2 f^2 + K^2 N^2}. \tag{4.20}$$

The denominator arises in the same way as the $m^2 f^2 + K^2N^2$ factor in the inertio-gravity wave dispersion relation. It will be captured as accurately as possible provided p is staggered with respect to w and, if K^2N^2 can be large, provided u and v are stored at the same levels as p and θ is stored at the same levels as w. The numerator will be captured accurately provided θ is stored at the same levels as w.

4.5.3.4 Numerical Dispersion Relations for Some Example Configurations

Figure 4.5 shows two plausible grid configurations that are natural extensions to the compressible Euler equations of the Lorenz and Charney–Phillips grids. According to our heuristic reasoning above, the Charney–Phillips grid should be as accurate as possible for all types of waves. This does indeed turn out to be the case; Fig. 4.6

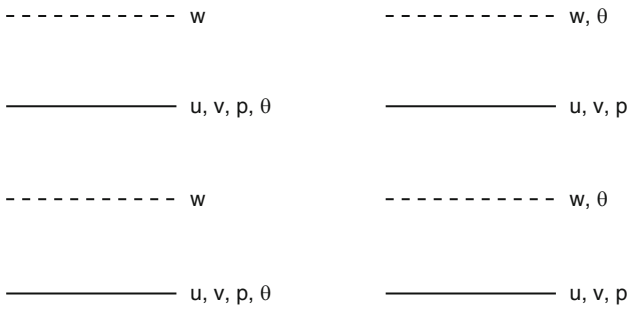

Fig. 4.5 Schematic showing the vertical arrangement of variables for compressible Euler versions of the Lorenz (*left*) and Charney–Phillips (*right*) grids

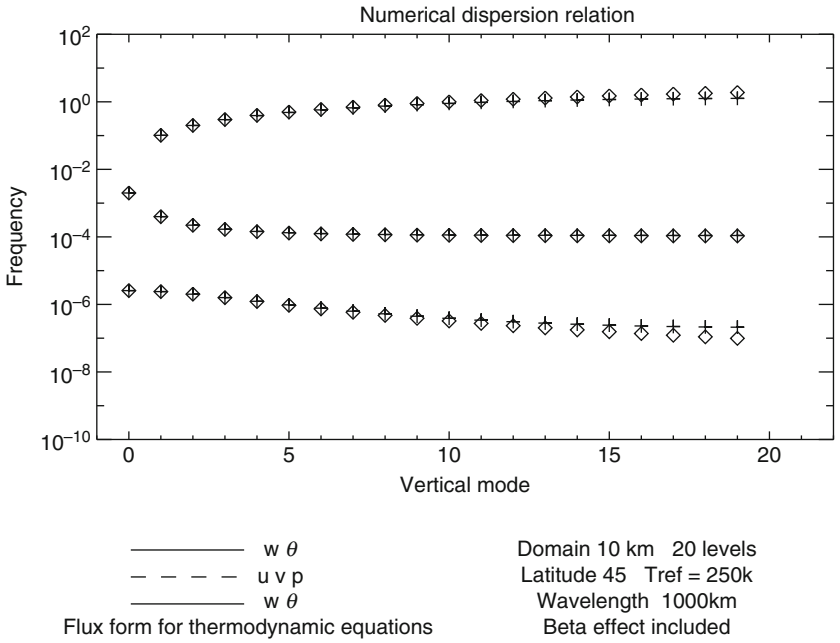

Fig. 4.6 Numerical dispersion relation for the optimal vertical configuration shown in the *right panel* of Fig. 4.5 (*crosses*) and exact dispersion relation (*diamonds*). The domain depth is 10^4 m with a rigid lid, horizontal wavelength is 1,000 km, and the geometry is that for a β-plane at 45°N. The reference state is resting and in hydrostatic balance with a uniform temperature of 250 K. The numerical dispersion relation was calculated for a uniform grid with 20 full-levels. The *upper curve* corresponds to internal acoustic modes, the *middle curve* corresponds to the external acoustic mode (mode number zero) and internal inertio-gravity modes, and the *lower curve* corresponds to Rossby modes. Only westward propagating modes are shown. There are also eastward propagating acoustic and inertio-gravity mode branches almost identical to the westward branches shown

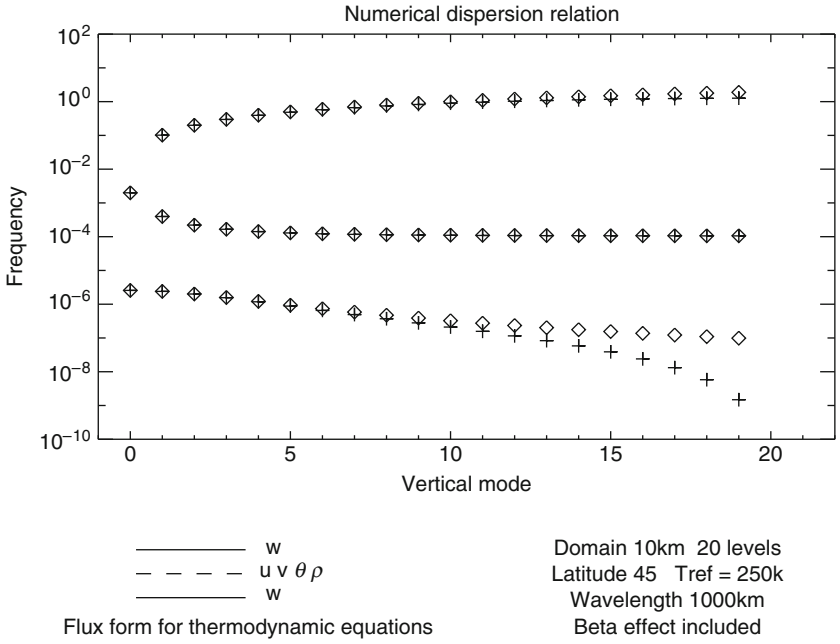

Fig. 4.7 As in Fig. 4.6 but for the vertical configuration shown in the *left panel* of Fig. 4.5

shows an example numerical dispersion relation, computed numerically, for this configuration.

The Lorenz grid should be accurate for acoustic and inertio-gravity waves provided K^2N^2 does not dominate m^2f^2. Figure 4.7 shows the numerical dispersion relation for this configuration when this condition holds. The acoustic and inertio-gravity wave dispersion relations are indeed captured accurately, but the Rossby modes are retarded (compare Fig. 4.6). Also, as in the hydrostatic case, the Lorenz grid supports a zero-frequency computational mode, which is not visible in Fig. 4.7.

There are some subtleties in exactly how the pressure gradient term should be evaluated, particularly if we wish to predict ρ rather than p to facilitate mass conservation (Thuburn 2006). Figure 4.8 shows the numerical dispersion relation when we predict ρ instead of p on the Charney–Phillips grid, assuming that the pressure gradient term is written as $(1/\rho)\nabla p$, discretized in the obvious way, with p diagnosed from ρ and a vertically averaged θ. In this calculation the buoyancy effect of θ is, in effect, vertically averaged, with the result that short-vertical-wavelength Rossby waves are retarded. Figure 4.9 shows the numerical dispersion relation for the same configuration if we use the alternative form $c_p\theta\nabla\Pi$ for the pressure gradient term, where c_p is the specific heat capacity at constant pressure and $\Pi = (p/p_0)^\kappa$. This calculation feels the full buoyancy effect of θ, and all waves are handled as accurately as possible.

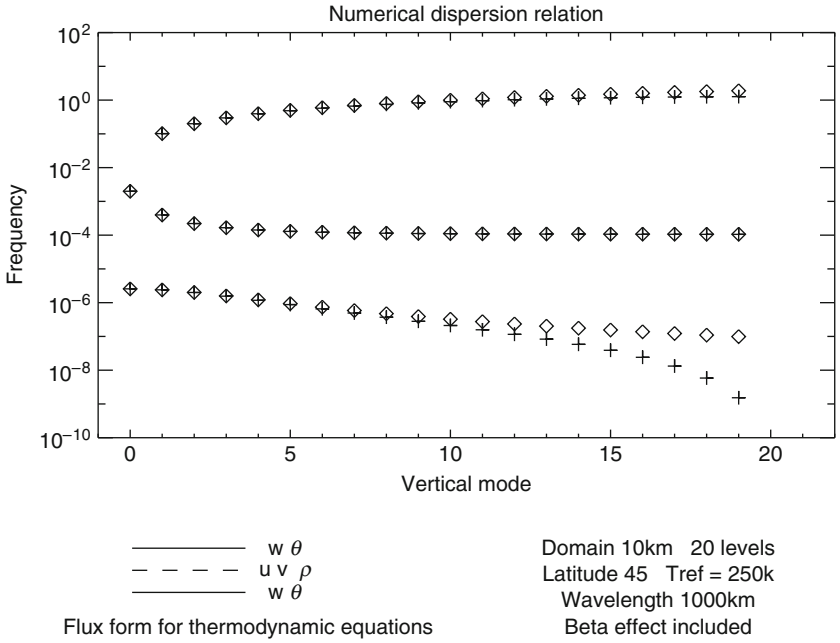

Fig. 4.8 As in Fig. 4.6 but for the vertical configuration predicting ρ instead of p and using the $(1/\rho)\nabla p$ form of the pressure gradient

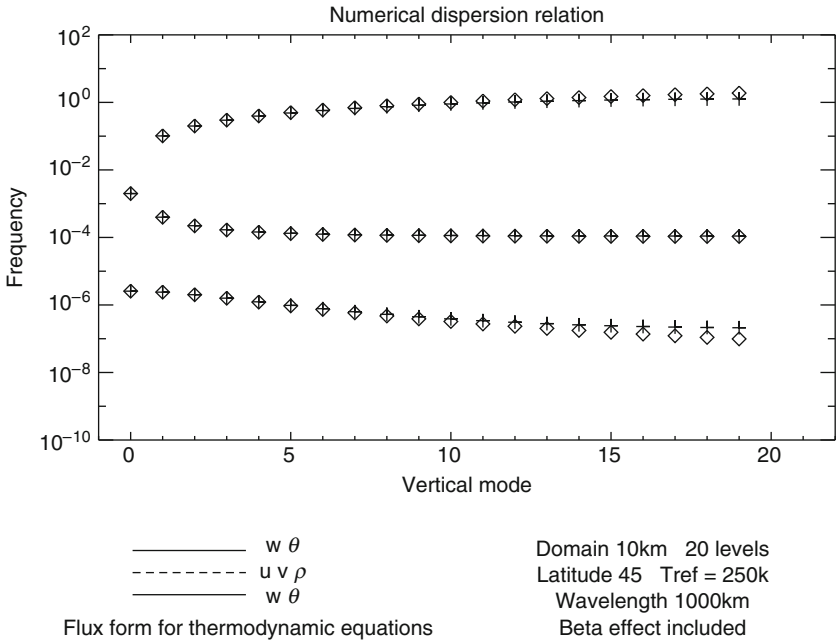

Fig. 4.9 As in Fig. 4.6 but for the vertical configuration predicting ρ instead of p and using the $c_p\theta\nabla\Pi$ form of the pressure gradient

4.6 Conclusion

The main choices of vertical coordinate have been introduced. They each have advantages and disadvantages, and indeed there is ongoing research and development pursuing several of the options.

Two of the main issues in the design of vertical discretizations are conservation properties and wave dispersion properties, and we have touched on both topics. Better wave dispersion properties can be obtained with the Charney–Phillips family of grids, particularly if careful attention is paid to the formulation of the pressure gradient term. On the other hand, conservation properties are more easily obtained using the Lorenz family of grids. There is ongoing debate over the relative importance of these two factors, and new models are being developed with both Charney–Phillips and Lorenz grids.

Incidentally, further issues and complexity arise when considering the coupling of the dynamical core to the physical parameterizations. For example, with a Charney–Phillips grid, should one store moisture at density levels, facilitating conservation of moisture, or at θ-levels, facilitating the calculation of important thermodynamic quantities like relative humidity? There is clearly great scope for further research.

References

Adcroft A, Hill C, Marshall J (1997) Representation of topography by shaved cells in a height coordinate ocean model. Mon Wea Rev 125:2293–2315

Arakawa A, Moorthi S (1988) Baroclinic instability in vertically discrete systems. J Atmos Sci 45:1688–1707

Charney JG, Phillips NA (1953) Numerical integration of the quasi-geostrophic equations for barotropic and simple baroclinic flow. J Meteorol 10:71–99

Durran DR (1999) Numerical Methods for Wave Equations in Geophysical Fluid Dynamics. Springer-Verlag

Gal-Chen T, Somerville RC (1975) On the use of a coordinate transformation for the solution of Navier-Stokes equations. J Comput Phys 17:209–228

Hsu YJG, Arakawa A (1990) Numerical modeling of the atmosphere with an isentropic vertical coordinate. Mon Wea Rev 118:1933–1959

Kasahara A (1974) Various vertical coordinate systems used for numerical weather prediction. Mon Wea Rev 102(7):509–522

Konor CS, Arakawa A (1997) Design of an atmospheric model based on a generalized vertical coordinate. Mon Wea Rev 125(7):1649–1673

Lin SJ (2004) A 'vertically Lagrangian' finite-volume dynamical core for global models. Mon Wea Rev 132:2293–2307

Lorenz EN (1960) Energy and numerical weather prediction. Tellus 12:364–373

Phillips NA (1957) A coordinate system having some special advantage for numerical forecasting. J Meteorol 14:184–185

Schneider EK (1987) An inconsistency in vertical discretization in some atmospheric models. Mon Wea Rev 115:2166–2169

Shaw TA, Shepherd TG (2007) Angular momentum conservation and gravity wave drag parametrization: Implications for climate models. J Atmos Sci 64:190–203

Simmons AJ, Burridge DM (1981) An energy and angular-momentum conserving vertical finite-difference scheme and hybrid vertical coordinates. Mon Wea Rev 109(4):758–766
Staniforth A, Wood N (2003) The deep-atmosphere Euler equations in a generalized vertical coordinate. Mon Wea Rev 131:1931–1938
Starr VP (1945) A quasi-Lagrangian system of hydrodynamical equations. J Atmos Sci 2:227–237
Thuburn J (2006) Vertical discretizations giving optimal representation of normal modes: Sensitivity to the form of the pressure gradient term. Quart J Roy Meteorol Soc 132:2809–2825
Thuburn J, Woollings TJ (2005) Vertical discretizations for compressible Euler equation atmospheric models giving optimal representation of normal modes. J Comput Phys 203:386–404
Tokioka T (1978) Some considerations on vertical differencing. J Meteorol Soc Japan 56:98–111